



Article

Structure, Luminescence, and Magnetic Properties of Crystalline Manganese Tungstate Doped with Rare Earth Ion

Jae-Young Jung ^{*}, Soung-Soo Yi, Dong-Hyun Hwang  and Chang-Sik Son

Division of Materials Science and Engineering, Silla University, Busan 46958, Korea; ssiyi@silla.ac.kr (S.-S.Y.); dhhwang@silla.ac.kr (D.-H.H.); csson@silla.ac.kr (C.-S.S.)

* Correspondence: eayoung21@naver.com; Tel.: +82-51-999-5465

Abstract: The precursor prepared by co-precipitation method was sintered at various temperatures to synthesize crystalline manganese tungstate (MnWO_4). Sintered MnWO_4 showed the best crystallinity at a sintering temperature of 800 °C. Rare earth ion (Dysprosium, Dy^{3+}) was added when preparing the precursor to enhance the magnetic and luminescent properties of crystalline MnWO_4 based on these sintering temperature conditions. As the amount of rare earth ions was changed, the magnetic and luminescent characteristics were enhanced; however, after 0.1 mol.%, the luminescent characteristics decreased due to the concentration quenching phenomenon. In addition, a composite was prepared by mixing MnWO_4 powder, with enhanced magnetism and luminescence properties due to the addition of dysprosium, with epoxy. To one of the two prepared composites a magnetic field was applied to induce alignment of the MnWO_4 particles. Aligned particles showed stronger luminescence than the composite sample prepared with unsorted particles. As a result of this, it was suggested that it can be used as phosphor and a photosensitizer by utilizing the magnetic and luminescent properties of the synthesized MnWO_4 powder with the addition of rare earth ions.

Keywords: MnWO_4 ; photoluminescence; co-precipitation; magnetic; synthesis



Citation: Jung, J.-Y.; Yi, S.-S.; Hwang, D.-H.; Son, C.-S. Structure, Luminescence, and Magnetic Properties of Crystalline Manganese Tungstate Doped with Rare Earth Ion. *Materials* **2021**, *14*, 3717. <https://doi.org/10.3390/ma14133717>

Academic Editors: Willem D. van Driel and Maryam Yazdan Mehr

Received: 3 June 2021

Accepted: 30 June 2021

Published: 2 July 2021

Publisher's Note: MDPI stays neutral with regard to jurisdictional claims in published maps and institutional affiliations.



Copyright: © 2021 by the authors. Licensee MDPI, Basel, Switzerland. This article is an open access article distributed under the terms and conditions of the Creative Commons Attribution (CC BY) license (<https://creativecommons.org/licenses/by/4.0/>).

1. Introduction

Recently, metal tungstate (MXO_4 , $M = \text{Ba, Ca, Mn, Sr}$, $X = \text{Mo, W}$) has attracted a lot of attention because of its applicability as a multiferroic, light-emitting material, light-emitting diode, and laser [1,2]. Among tungstate materials, the tetragonal scheelite-like structure is a comportsing phosphor host material and photocatalytic material because the WO_4^{2-} group shows a good absorption rate in the ultraviolet (UV) and blue ranges. This produces a specific emission band through energy transfer from the WO_4^{2-} group to the RE ion [3–5]. In particular, manganese tungstate (MnWO_4) crystal is a suitable parent material for doping rare earth and metal ions because of its excellent thermal stability and high energy transfer efficiency from tungsten ions to activator ions; also, rare earth and metal ions are generated by energy transfer between 4f-4f shells [6]. This material has the advantage of generating a high emission intensity with a narrow band gap and a variety of emission wavelengths [7]. The kind and positional symmetry of the activator ions doped in the thermally and chemically stable parent grid are important factors in implementing various types of electrochemical, laser, multiferroic, and display devices [8,9]. The diversity of the MnWO_4 depends on the type and concentration of activator ions, the sintering temperature, the size of the crystal grain, and the synthesis conditions. Martinez et al. proposed that MWO_4 ($M = \text{Ni, Co, Mn, Cu}$) can be synthesized using the dissolution-precipitation method and applied to the photocatalytic evaluation field through structural and UV absorbance characteristics analysis [10]. Li et al. synthesized MnWO_4 nanoparticles using co-precipitation and suggested that electrochemical capacitive performance could be investigated by galvanostatic charge/discharge (GV), cycle electrochemical impedance spectroscopy (EIS), and cyclic voltammetry (CV) [11]. It has been reported that by changing

the amount of and type of rare earth ions added by changing the structure and luminescence properties of BaWO_4 , it is possible to synthesize a phosphor with good crystallinity and capable of implementing various colors using the co-precipitation method [10]. In addition, the $\text{BaWO}_4 \cdot \text{Ln}^{3+}$ ($\text{Ln} = \text{Eu}, \text{Tb}, \text{and Dy}$) powders synthesized via a solid-state reaction, which showed green, yellow, and red emissions [12]. As in the previous literature, various synthesis methods and application cases of tungstate materials have been reported. In this study, the MnWO_4 precursor was prepared using the co-precipitation method and the optimum synthesis temperature was investigated by varying the sintering temperature. In addition, it was suggested that magnetic and luminescent properties can be realized through the addition of rare earth ions, and that MnWO_4 can be applied as a fluorescent and photosensitizing material.

2. Materials and Methods

2.1. Synthesis of MnWO_4 and Rare Earth Doped with MnWO_4

Materials: manganese (II) nitrate ($\text{Mn}(\text{NO}_3)_2 \cdot x\text{H}_2\text{O}$), sodium tungstate (Na_2WO_4), dysprosium (III) nitrate ($\text{Dy}(\text{NO}_3)_3 \cdot x\text{H}_2\text{O}$, Dy^{3+}), and Allied epoxy set were used in this study.

First, two beakers 'A' and 'B' were prepared. In beaker 'A', 1 mmol of $\text{Mn}(\text{NO}_3)_2 \cdot x\text{H}_2\text{O}$ was added to 50 mL of distilled water (D.I water) and stirred until completely dissolved. In beaker 'B', 50 mL of distilled water was added with the same moles of Na_2WO_4 and stirred until dissolved. When reagents in both beakers had dissolved, beaker 'B' solution was slowly poured into stirring beaker 'A' and stirred for about 30 min. After that, powder was obtained using a centrifuge, and the precursor was prepared by rinsing with D.I water twice to remove the remaining sodium. The prepared precursors were dried in an 80 °C oven for about 18 h. The dried precursors were heat-treated at various sintering temperatures (80, 400, 600, 800, 900, and 1000 °C) and then structural characteristics were investigated. In addition, to synthesize MnWO_4 having magnetic and luminescent properties in the same manner, $\text{MnWO}_4 \cdot \text{Dy}^{3+}$ powder was synthesized by varying the amount of $\text{Dy}(\text{NO}_3)_3 \cdot x\text{H}_2\text{O}$ added to beaker 'A' when preparing the precursor, as shown in Figure 1.

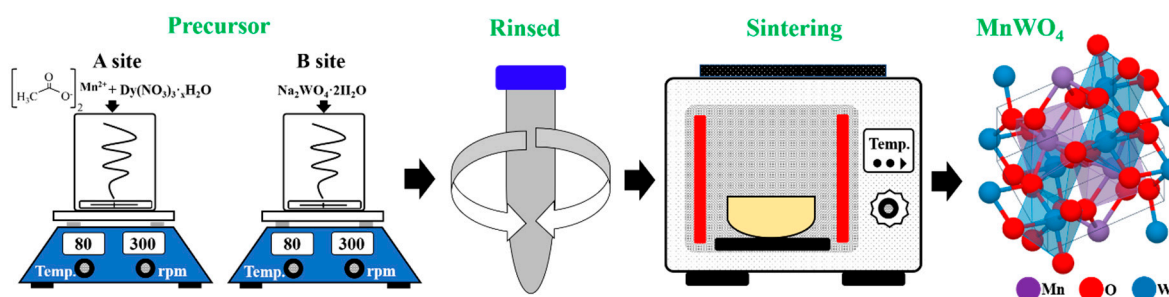


Figure 1. Schematic of MnWO_4 powder synthesis experimental procedure.

2.2. Characterization

The structural properties of the MnWO_4 and $\text{MnWO}_4 \cdot \text{Dy}^{3+}$ powders were obtained by X-ray diffraction analysis (XRD; Rigaku Ultima IV, Tokyo, Japan). Raman spectra were obtained using a Raman spectrometer (LabRam-HR 800, Horiba Jobin-Yvon, France), equipped with a 514 nm laser as excitation source. The magnetic properties of the samples were measured using a vibrating sample magnetometer with MnWO_4 and $\text{MnWO}_4 \cdot \text{Dy}^{3+}$ samples after magnetization with 6 T pulsing magnetic field. The chemical composition and oxidation state of the synthesized phosphors were investigated by X-ray photoelectron spectroscopy (XPS, ESCALAB 250XI, Waltham, MA, USA). The peak position of the insulating samples was calibrated using a C1 of 285 eV. The surface morphology and microstructure were observed by field emission scanning electron microscopy (FE-SEM, SU-8220, Hitachi, Tokyo, Japan) and transmission electron microscopy (TEM, JEM 2100F,

JEOL, Japan). Photoluminescence spectra were obtained through a photomultiplier tube operating at 250 V, a fluorescence spectrophotometer (Scinco, FS-2, Seoul, Korea), and an optical microscope (OM, BX53M, OLYMPUS, Shinjuku, Japan).

2.3. Fabrication of $\text{MnWO}_4\text{:Dy}^{3+}$ Epoxy Composite

A composite was prepared by mixing with epoxy to find changes in the luminescence properties of MnWO_4 particles aligned by magnetic field influence. An epoxy resin and a hardener were prepared at a weight ratio of 10:1, and 3 wt.% of $\text{MnWO}_4\text{:Dy}^{3+}$ powder was added and stirred for 1 h. The mixture was poured into a mold and air bubbles were removed in a vacuum desiccator for 1 h. After that, one specimen was hardened as is; the other specimen was hardened by generating a magnetic field by installing magnets on both sides of the mold to align the $\text{MnWO}_4\text{:Dy}^{3+}$ particles.

3. Results and Discussion

3.1. Crystallinity of MnWO_4 According to Various Sintering Temperatures

The precursor prepared by co-precipitation method was heat-treated at various temperatures to determine the crystallinity and structure of the synthesized MnWO_4 , followed by XRD analysis, with results as shown in Figure 2a. A clear XRD pattern could not be confirmed at relatively low heat treatment temperature, but it was found that MnWO_4 could be synthesized even at low temperature. At the heat treatment temperature of 600 °C, crystalline MnWO_4 was confirmed, as in the results of the International Center for Diffraction Data (ICDD 01-080-0133, monoclinic, P2/c) reference. In particular, main peaks of the (111), (011), (002), and (130) phases were identified [13]. In addition, as the sintering temperature increased, the full width at half maximum (FWHM) of the main peaks decreased and showed a tendency to decrease significantly at 800 °C (Figure 2b). As a result of this, it is thought that the increase of the sintering temperature increases the crystallinity of MnWO_4 [14]. However, there was no significant change after the sintering temperature of 800 °C and, for energy saving, the optimum sintering temperature was determined to be 800 °C.

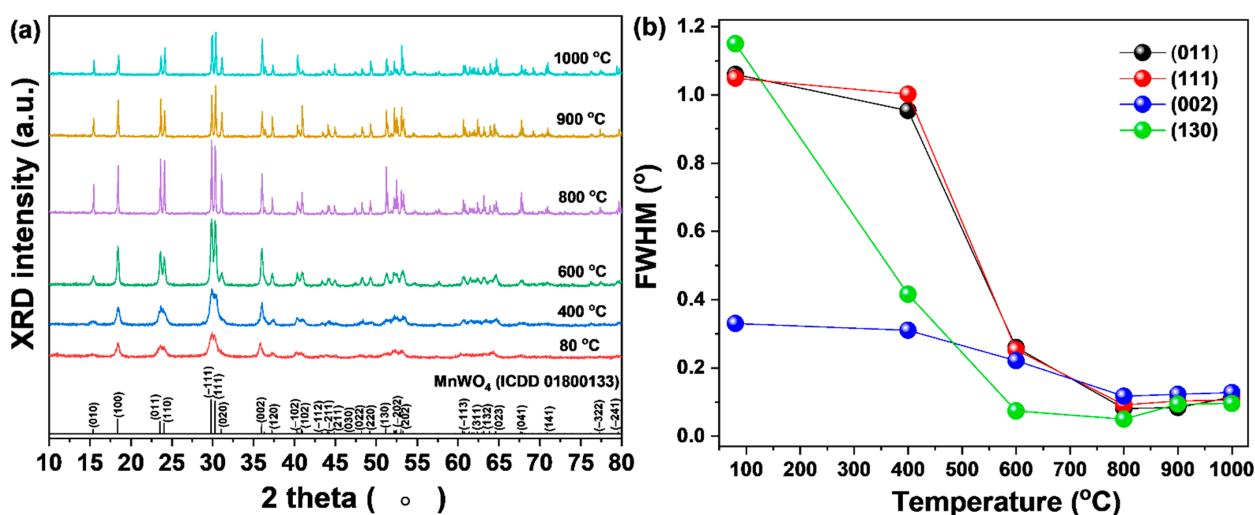


Figure 2. (a) XRD patterns of MnWO_4 and (b) FWHM of main peaks according to various sintering temperatures.

3.2. Crystallinity, and Magnetic and Chemical State of MnWO_4 Doped with Dy^{3+} Ions

To observe changes in the characteristics of MnWO_4 with the addition of rare earth materials, precursors were prepared by changing the amounts of dysprosium ions (Dy^{3+} ; 0.05, 0.1, 0.25, 0.5, 0.7, 1, 1.25 mol.%) added in the process of preparing the precursor by the same experimental method. The prepared precursor was sintered at 800 °C. When the added amount of Dy^{3+} ions was small (0.1 mol.%), the main peaks of the (−111),

(011), (002), and (130) phases of the FWHM tended to increase. This is thought to be a phenomenon caused by the addition to the lattice of rare earth ions with relatively large ionic radii. In addition, when the amount of added rare earth material was 0.25 mol.%, the FWHM decreased (Figure 3b), which is thought to have the effect of enhancing the crystallinity [15]. However, as the amount of rare earth ions increased, the FWHM and secondary phase were found. The secondary phase (Figure 3a, black diamond symbol) was identified as a dysprosium oxide phase. When the added amount of rare earth ions was 0.25 mol.% or more, the crystallinity of MnWO_4 decreased and a secondary phase formed; the critical doping concentration was considered to be 0.25 mol.%.

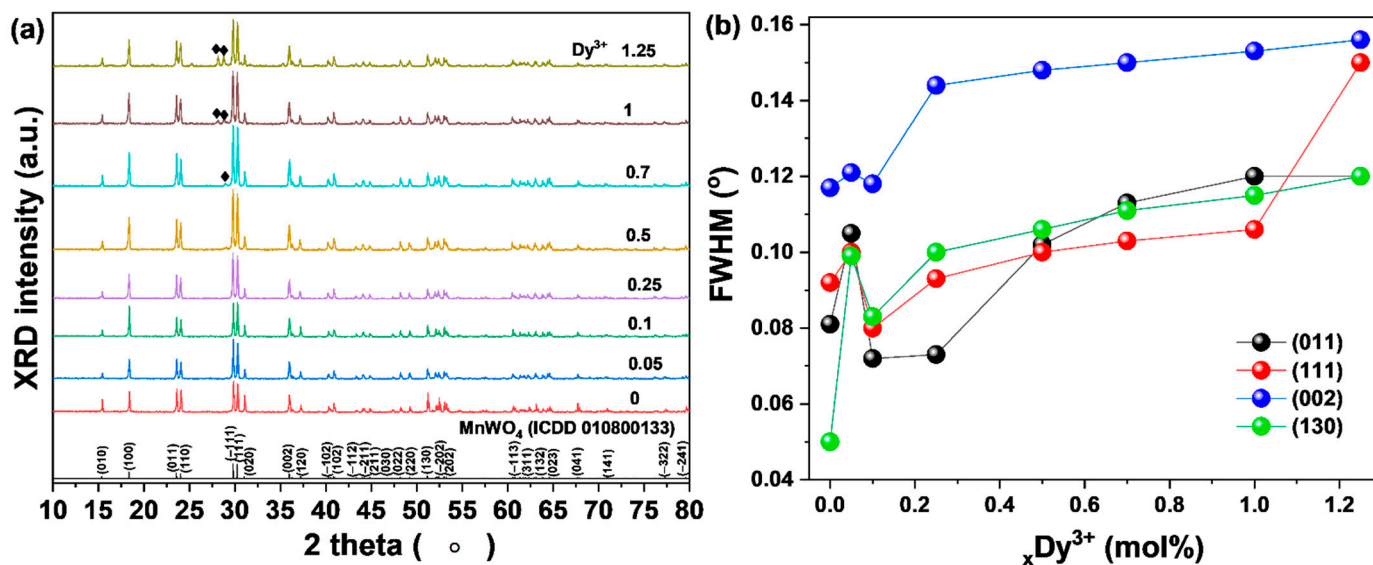


Figure 3. (a) XRD patterns of $\text{MnWO}_4:\text{Dy}^{3+}$ and (b) change of FWHM.

Raman analysis was performed to double check the XRD data obtained for Dy^{3+} ion-doped crystalline MnWO_4 . The vibration bands of MnWO_4 shown in Figure 4a show six Raman active modes at 200, 320, 391, 539, 691, and 878 cm^{-1} . This may be due to the $\nu(\text{A}_g)$, $\nu(\text{B}_g)$, $\delta(\text{A}_g)$, symmetric A_g , $(\text{W}_2\text{O}_4)_n$ chain, $\nu_{\text{as}}(\text{B}_g)$ of the Mn cation, and the symmetric A_g oscillations of the two terminal WO groups, respectively. There is crystalline MnWO_4 , which correlates accurately with the literature [16]. The very strong band appearing at 878 cm^{-1} corresponds to the strong symmetrical stretching of the WO_2 group in MnWO_4 . The bands at 769 and 691 cm^{-1} indicate the existence of weak asymmetric and symmetric tensile vibration modes of W-O-W bonds [17]. The peak at 539 cm^{-1} is attributed to the tensile vibration of Mn-O [18]. The band at 391 cm^{-1} indicates that there is a symmetric stretch of W-O-W [19]. The band at 320 cm^{-1} checked the moderate shear of WO_2 and W-O-W [20]. The weak vibrating band appears at 251 cm^{-1} , indicating the bending mode of $[\text{WO}_6]_6$ and the twisting vibrating mode of the WO_2 group [21]. The two vibrating bands at 158 and 121 cm^{-1} are translational modes of tungsten [22]. In Raman analysis, no significant change was observed between the $\text{MnWO}_4:\text{Dy}^{3+}$ and MnWO_4 samples. To identify changes in the magnetic properties according to the amount of Dy^{3+} added to the synthesized crystalline MnWO_4 , vibrating sample magnetometer (VSM) analysis was performed (Figure 4b).

In addition, it was shown that the magnetic properties increased as the amount of added Dy^{3+} ions increased. Due to its 4f orbital, the Dy^{3+} ion is a prototype of a highly correlated electronic system. It is partially occupied by the f shell, and the 4f orbital is split into seven non-degenerate orbitals. According to Hund's law, the magnetic moments are caused by the 4f and 5d orbitals, which are consistent with the magnetic moments of the corresponding Dy^{3+} ions [23].

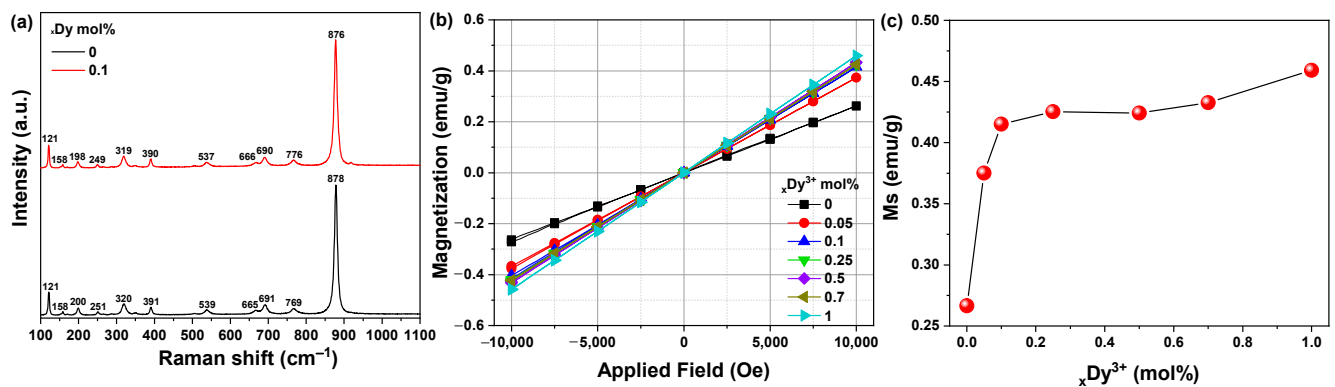


Figure 4. (a) Raman shift of MnWO₄ and MnWO₄:Dy³⁺, (b) magnetization properties of MnWO₄:Dy³⁺ performed at room temperature, and (c) scale of M(10 kOe) vs. Dy³⁺ ions content.

To determine MnWO₄:Dy³⁺ samples of binding energy, oxidation, and chemical state, XPS analysis was performed on MnWO₄:Dy³⁺ (Figure 5). Results show Mn 2p; two peaks can be observed corresponding to Mn 2p_{3/2} and Mn 2p_{1/2} at 641 eV and 653 eV, respectively. This indicates that the Mn present in the sample is in +2 oxidation state [24]. The XPS spectrum of W 4f is shown in Figure 5b. It has two peaks, corresponding to W 4f_{7/2} and W 4f_{5/2} at 34.88 and 36.98 eV, respectively. The W 4f_{7/2} and W 4f_{5/2} doublets' spin-orbit is at 2.1 eV, and the oxidation state of W can be specified as +6 [25]. The O 1s peak shows a main component with a central energy of 530 eV and a lower binding energy, which monitored to the formation of O₂ oxide-coupled manganese and tungsten elements (Mn–O–W), as shown in Figure 5c. In Figure 5e, the RE³⁺ 3d spectrum can be observed for the MnWO₄ sample doped with RE³⁺. The Dy³⁺ 3d spectrum is visible at 1317 eV and 1335 eV; these can be assigned to the RE³⁺ 3d_{5/2} and 3d_{3/2} states, respectively, based on the Dy–O bond [26].

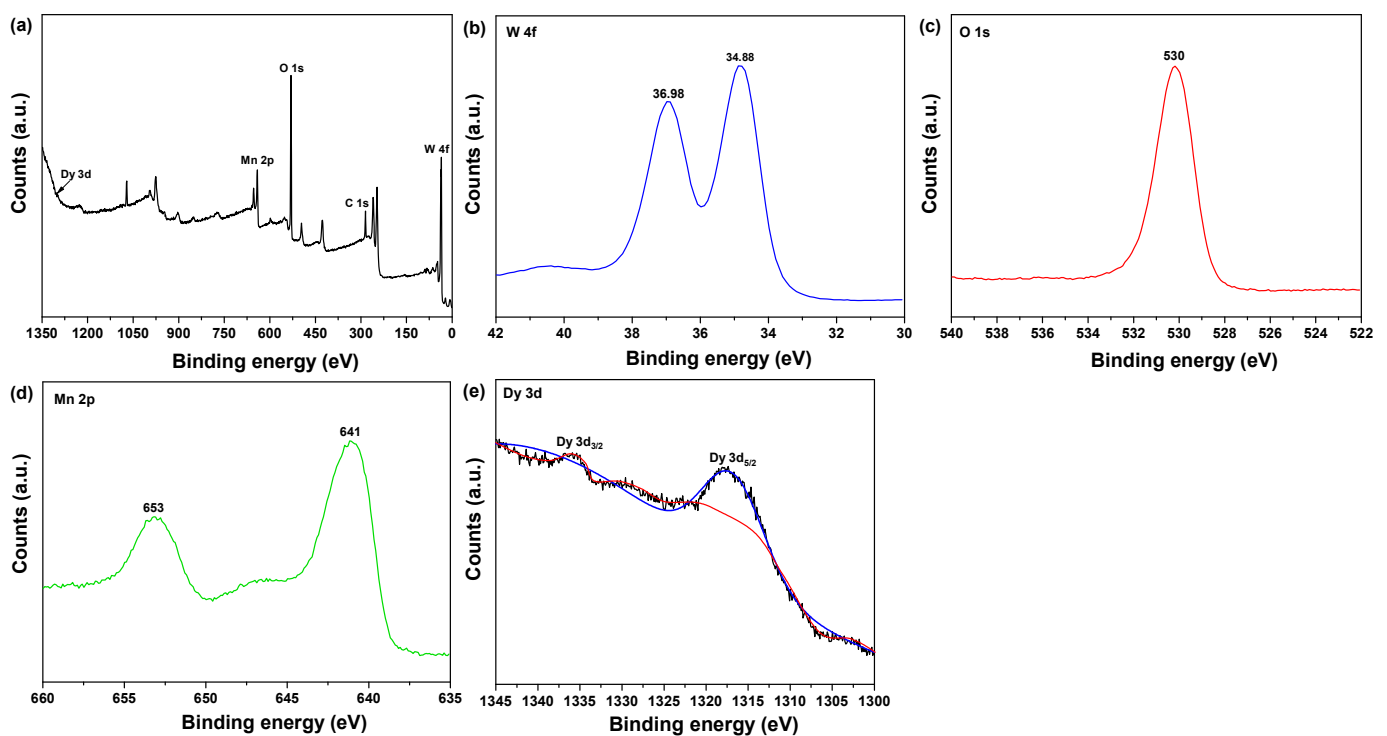


Figure 5. XPS data of MnWO₄:Dy³⁺: (a) survey, (b) W 4f, (c) O 1s, (d) Mn 2p, and (e) Dy 3d.

3.3. Luminescence and Morphology Properties of MnWO₄ Doped with Dy³⁺ Ions

The photoluminescence excitation (PLE) and photoluminescence (PL) spectra of MnWO₄:Dy³⁺ powder synthesized with activator Dy³⁺ ions of different doping concentrations were obtained. The excitation spectrum monitored at 575 nm consists of peaks in the range of 200 to 400 nm. The PLE spectrum almost covers the ultraviolet region. The excitation band is wide in the range of 270–300 nm to 286 nm, corresponding to the Dy³⁺-O²⁻ charge transfer band (CTB) in the matrix crystal [27,28]. When the concentration of Dy³⁺ increased from 0.05 to 0.25 mol.%, the intensity of all excitation bands increased rapidly, reaching a maximum at 0.1 mol.%, and then decreased significantly within the Dy³⁺ concentration range of 0.5 to 1.25 mol.%, as shown in Figure 6a. For MnWO₄:Dy³⁺ powder, the emission spectrum under 286 nm excitation shows two main emission bands at 480 and 575 nm, corresponding to the ⁴F_{9/2} → ⁶H_{15/2} magnetic dipole (MD) transition and the transition of the electric dipole (ED) of ⁴F_{9/2} → ⁶H_{13/2}, respectively. [29] The emission intensity at 575 nm (ED) is very obvious. This result shows that when Dy³⁺ concentration is 0.1 mol.%, the position of the Dy³⁺ ion in the MnWO₄ host lattice shifts from a non-antisymmetric position to an antisymmetric position. Among all the emission transitions of Dy³⁺, the strongest yellow emission originated from the ⁴F_{9/2} → ⁶H_{13/2} ED transition. As the concentration of Dy³⁺ ions increased from 0.5 to 1.25 mol.%, the intensity of the main ⁴F_{9/2} → ⁶H_{13/2} transition rapidly decreased due to the concentration quenching effect (Figure 6c), mainly due to non-radiant energy transfer between Dy³⁺ activator ions. The critical distance R_c between the Dy³⁺ activator ions can be calculated using the following equation presented by Blasse [30],

$$R_c = 2(3V/4\pi \chi_c Z)^{1/3} \quad (1)$$

where V is the volume of the unit cell, X_c is the critical concentration (Dy³⁺ ions), and Z is the number of host cations in the unit cell. For the MnWO₄ host, $V = 146.299 \text{ \AA}^3$, $x_c = 0.1$ and $Z = 2$. Therefore, R_c was estimated to be about 11.65 Å. It is well known that there are three types of interactions in which electric multipolar interaction is involved in the energy transfer: dipole–dipole, dipole–quadrupole, and quadrupole–quadrupole interactions.

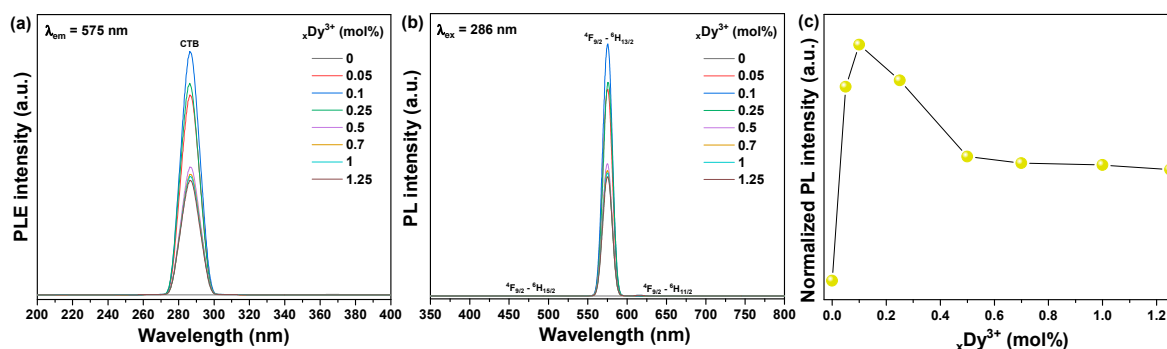


Figure 6. Luminescence properties of MnWO₄:Dy³⁺: (a) PLE spectra under 575 nm, (b) PL spectra under 286 nm, and (c) integrated PL intensity.

To observe the shape and morphology of the synthesized MnWO₄:Dy³⁺ particles, FE-SEM and TEM analyses were performed and results are shown in Figure 7. MnWO₄:Dy³⁺ was generally clustered in the shape of a long, round column in the vertical direction; the size was about 4 μm in length and about 2 μm in width. In high-resolution analysis using TEM, the interplanar distance of the (−111) phase was observed to be about 0.213 nm. This was similar to the value calculated from the XRD data ($d_{(-111)}$ spacing; 0.299 nm). In addition, Mn, W, O, and Dy were detected in EDX component analysis; components of synthesized MnWO₄:Dy³⁺ were confirmed.

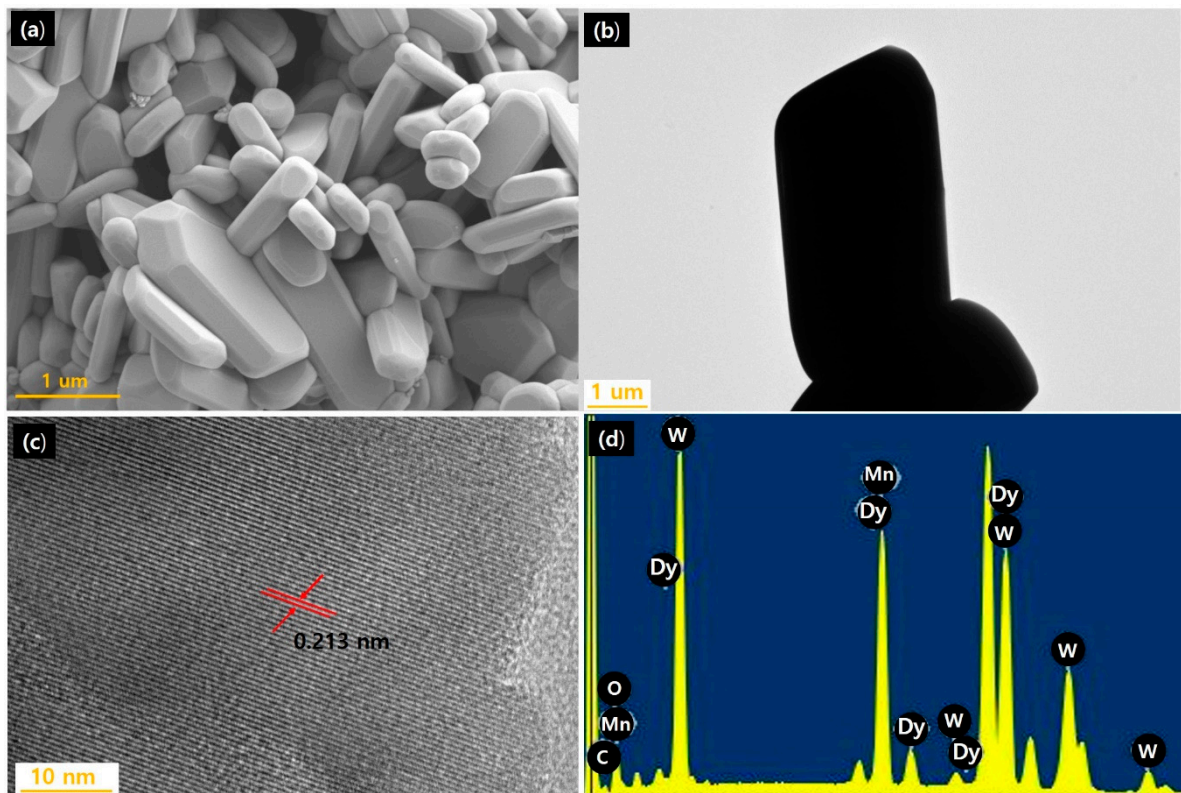


Figure 7. (a) SEM image of $\text{MnWO}_4:\text{Dy}^{3+}$, (b) TEM image of $\text{MnWO}_4:\text{Dy}^{3+}$, (c) high-resolution image, and (d) EDX composition analysis result.

3.4. $\text{MnWO}_4:\text{Dy}^{3+}$ Particle Aligned in Epoxy Composite by Magnetic Field

As can be seen in Figure 8a, the synthesized $\text{MnWO}_4:\text{Dy}^{3+}$ powder was dispersed in ethanol and then a magnet was installed. It was confirmed that the powders moved in the direction of the magnet and can be used as a paramagnetic material. In addition, movements of particles in the mixture made with epoxy polymer were observed through an optical microscope according to the presence or absence of a magnetic field (Figure 8b). $\text{MnWO}_4:\text{Dy}^{3+}$ particles were confirmed to align in the direction of the magnetic field. Using these characteristics, we made an epoxy composite and investigated changes in luminescence characteristics according to alignment of particles according to presence or absence of magnetic field (Figure 8c). The composite in which the particles were aligned by exposure to the magnetic field showed a strong luminescence intensity of about 10% (Figure 8d). This is thought to be a phenomenon that occurs because the energy transfer of the aligned particles works slightly more efficiently than in particles in which light energy introduced from the outside is agglomerated. It seems that, utilizing these characteristics, this material can be applied to fields such as display and medical engineering.

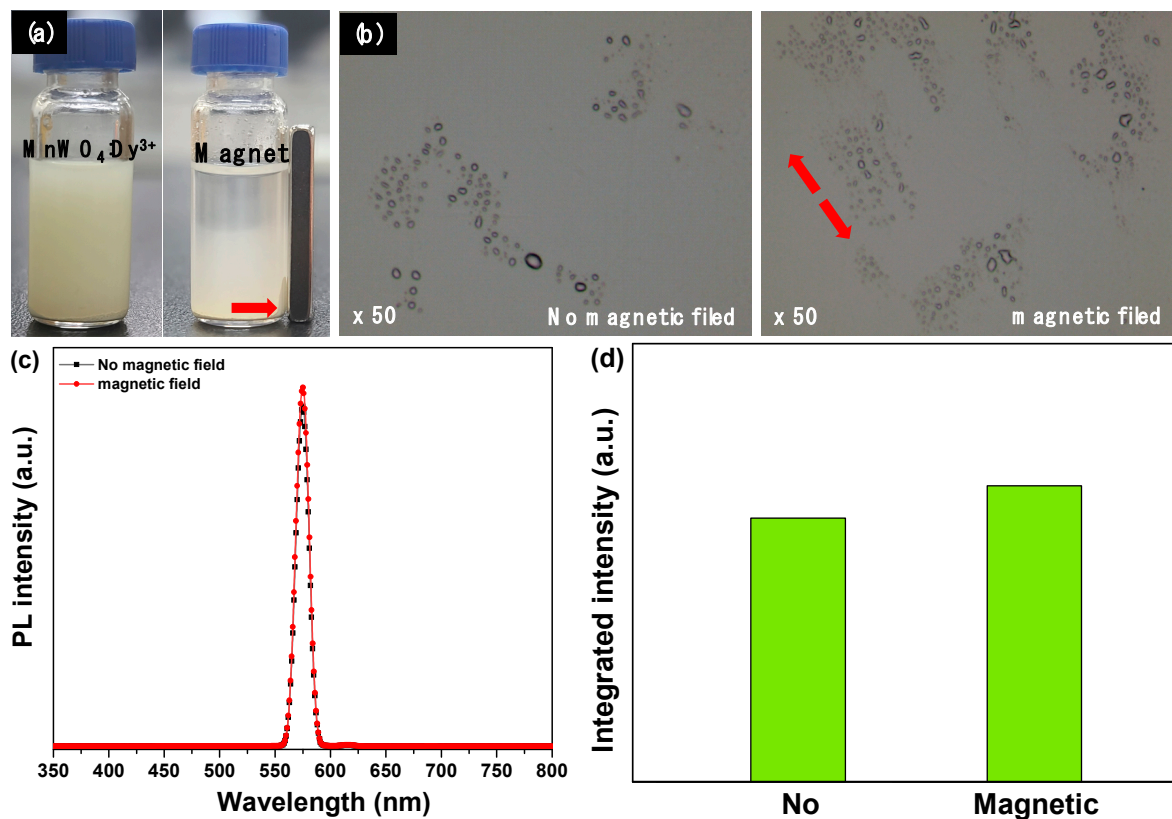


Figure 8. (a) Photograph of $\text{MnWO}_4:\text{Dy}^{3+}$ powder moved to magnet in ethanol, (b) OM images of $\text{MnWO}_4:\text{Dy}^{3+}$ particle behavior with magnetic field, (c) PL spectra, and (d) integrated PL intensity with magnetic field.

4. Conclusions

We propose that MnWO_4 powder synthesis is possible in an easy way. After preparing the MnWO_4 precursor using the co-precipitation method, the crystallinity change of MnWO_4 according to various synthesis temperatures was observed. The best crystallinity was exhibited when the heat treatment temperature was 800 °C. At this time, dysprosium, a rare earth ion, was added to enhance light emission and magnetic properties to synthesize $\text{MnWO}_4:\text{Dy}^{3+}$. According to the amount of Dy^{3+} ions added, the magnetic properties were enhanced and the luminescence properties were enhanced. When producing an epoxy composite using these properties, it was found that the luminescent properties were enhanced by about 10% as the particles were aligned in the magnetic field direction. It was suggested that the synthesized $\text{MnWO}_4:\text{Dy}^{3+}$ powder can be used as a paramagnetic material and can be applied to display and medical industries.

Author Contributions: Conceptualization, J.-Y.J.; D.-H.H.; methodology, J.-Y.J.; C.-S.S.; formal analysis, J.-Y.J., and D.-H.H.; investigation, J.-Y.J., and S.-S.Y.; writing—original draft preparation, J.-Y.J.; writing—review and editing, J.-Y.J., S.-S.Y., D.-H.H., and C.-S.S.; visualization, J.-Y.J.; supervision, J.-Y.J.; D.-H.H.; project administration, J.-Y.J., C.-S.S. All authors have read and agreed to the published version of the manuscript.

Funding: This research was supported by Basic Science Research Program through the National Research Foundation of Korea (NRF) funded by the Ministry of Education (grant number) (NRF-2019R1A6A3A01095400) and (NRF-2020R1F1A1072616) and by the National Research Foundation of Korea (NRF) grant funded by the Korea government (MSIT) (No. NRF-2018R1A5A1025594).

Institutional Review Board Statement: Not applicable.

Informed Consent Statement: Not applicable.

Data Availability Statement: The data presented in this study are available in the database of the authors at the Faculty of Materials Science and Engineering.

Conflicts of Interest: The authors declare no conflict of interest.

References

1. Downing, E.; Hesselink, L.; Ralston, J.; Macfarlane, R. A Three-Color, Solid-State, Three-Dimensional Display. *Science* **1996**, *273*, 1185–1189. [[CrossRef](#)]
2. Cooper, T.; De Leeuw, N. A combined ab initio and atomistic simulation study of the surface and interfacial structures and energies of hydrated scheelite: Introducing a CaWO₄ potential model. *Surf. Sci.* **2003**, *531*, 159–176. [[CrossRef](#)]
3. Nivetha, P.; Kavitha, B.; Kalanithi, M. Investigation of photocatalytic and antimicrobial activities of BaWO₄–MoS₂ nanoflowers. *J. Sci. Adv. Mater. Devices* **2021**, *6*, 65–74. [[CrossRef](#)]
4. Kuzmin, A.; Purans, J. Local atomic and electronic structure of tungsten ions in AWO₄ crystals of scheelite and wolframite types. *Radiat. Meas.* **2001**, *33*, 583–586. [[CrossRef](#)]
5. Koepke, C.; Wojtowicz, A.J.; Lempicki, A. Luminescence Excited-state absorption in excimer-pumped CaWO₄ crystals. *J. Lumin.* **1993**, *54*, 345–355. [[CrossRef](#)]
6. Grobelna, B.; Lipowska, B.; Klonkowski, A.M. Energy transfer in calcium tungstate doped with Eu(III) or Tb(III) ions incorporated into silica xerogel. *J. Alloys Compd.* **2006**, *419*, 191–196. [[CrossRef](#)]
7. Naik, S.; Salker, A. Solid state studies on cobalt and copper tungstates nano materials. *Solid State Sci.* **2010**, *12*, 2065–2072. [[CrossRef](#)]
8. Rajagopal, S.; Nataraj, D.; Mangalaraj, D.; Djaoued, Y.; Robichaud, J.; Khyzhun, O.Y. Controlled Growth of WO₃ Nanostructures with Three Different Morphologies and Their Structural, Optical, and Photodecomposition Studies. *Nanoscale Res. Lett.* **2009**, *4*, 1335–1342. [[CrossRef](#)]
9. López, X.A.; Fuentes, A.F.; Zaragoza, M.M.; Guillén, J.A.D.; Gutiérrez, J.S.; Ortiz, A.L.; Collins-Martínez, V. Synthesis, characterization and photocatalytic evaluation of MWO₄ (M = Ni, Co, Cu and Mn) tungstates. *Int. J. Hydrogen Energy* **2016**, *41*, 23312–23317. [[CrossRef](#)]
10. Li, F.; Xu, X.; Huo, J.; Wang, W. A simple synthesis of MnWO₄ nanoparticles as a novel energy storage material. *Mater. Chem. Phys.* **2015**, *167*, 22–27. [[CrossRef](#)]
11. Jung, J.-Y.; Kim, J.; Shim, Y.-S.; Hwang, D.; Son, C. Structure and Photoluminescence Properties of Rare-Earth (Dy³⁺, Tb³⁺, Sm³⁺)-Doped BaWO₄ Phosphors Synthesized via Co-Precipitation for Anti-Counterfeiting. *Materials* **2020**, *13*, 4165. [[CrossRef](#)] [[PubMed](#)]
12. Sun, X.; Sun, X.; Li, X.; He, J.; Wang, B. Synthesis and Luminescence of BaWO₄:Ln³⁺ (Ln = Eu, Tb, and Dy) Powders. *J. Electron. Mater.* **2014**, *43*, 3534–3538. [[CrossRef](#)]
13. Chen, S.; Chen, X.; Xue, Z.; Zhou, J.; Li, J.; Hong, J.; You, X. Morphology control of MnWO₄ nanocrystals by a solvothermal route. *J. Mat. Chem.* **2003**, *13*, 1132–1135. [[CrossRef](#)]
14. Shen, Y.-J.; Zhang, Y.; Gao, F.; Yang, G.-S.; Lai, X.-P. Influence of Temperature on the Microstructure Deterioration of Sandstone. *Energies* **2018**, *11*, 1753. [[CrossRef](#)]
15. Akhtar, M.N.; Hussain, T.; Khan, M.A.; Ahmad, M. Structural, magnetic, dielectric and high frequency response of synthesized rare earth doped bismuth nano garnets (BIG). *Results Phys.* **2018**, *10*, 784–793. [[CrossRef](#)]
16. Tanaka, T.; Hirai, H.; Matsuoka, T.; Ohishi, Y.; Yagi, T.; Ohtake, M.; Yamamoto, Y.; Nakano, S.; Irifune, T. Phase changes of filled ice Ih methane hydrate under low temperature and high pressure. *J. Chem. Phys.* **2013**, *139*, 104701. [[CrossRef](#)]
17. Dai, R.; Ding, X.; Wang, Z.; Zhang, Z. Pressure and temperature dependence of Raman scattering of MnWO₄. *Chem. Phys. Lett.* **2013**, *586*, 76–80. [[CrossRef](#)]
18. Iliev, M.; Gospodinov, M.M.; Litvinchuk, A.P. Raman spectroscopy of MnWO₄. *Phys. Rev. B* **2009**, *80*, 212302. [[CrossRef](#)]
19. Maczka, M.; Ptak, M.; Da Silva, K.P.; Freire, P.D.T.C.; Hanuza, J. High-pressure Raman scattering and anharmonicity study of multiferroic wolframite-type Mn_{0.97}Fe_{0.03}WO₄. *J. Physics Condens. Matter* **2012**, *24*, 345403. [[CrossRef](#)] [[PubMed](#)]
20. Ruiz-Fuertes, J.; Friedrich, A.; Gomis, O.; Errandonea, D.; Morgenroth, W.; Sans, J.A.; Santamaria-Perez, D. High-pressure structural phase transition in MnWO₄. *Phys. Rev. B* **2015**, *91*, 104109. [[CrossRef](#)]
21. Macavei, J.; Schulz, H. The crystal structure of wolframite type tungstates at high pressure. *Z. Krist. Cryst. Mater.* **1993**, *207*, 193–208. [[CrossRef](#)]
22. Iliev, M.N.; Guo, H.; Gupta, A. Raman spectroscopy evidence of strong spin-phonon coupling in epitaxial thin films of the double perovskite La₂NiMnO₆. *Appl. Phys. Lett.* **2007**, *90*, 151914. [[CrossRef](#)]
23. Chen, X.-Y.; Long, M.-Q.; Wang, Y.-P. Paramagnetic phases of two-dimensional magnetic materials. *Phys. Rev. B* **2020**, *102*, 214417. [[CrossRef](#)]
24. Jiang, F.; Pang, Z.; Yuan, H.; Wei, Z.; Xie, W.; Wu, Z.; Han, S. Room temperature ferromagnetic properties of dysprosium-doped tris(8-hydroxyquinoline) aluminum: Experimental and theoretical investigation. *RSC Adv.* **2016**, *6*, 43780–43785. [[CrossRef](#)]
25. Muthamizh, S.; Suresh, R.; Giribabu, K.; Manigandan, R.; Kumar, S.P.; Munusamy, S.; Narayanan, V. MnWO₄ nanocapsules: Synthesis, characterization and its electrochemical sensing property. *J. Alloys Compd.* **2015**, *619*, 601–609. [[CrossRef](#)]
26. Dong, F.; Sattayasamitsathit, S.; Zhang, Y.X.; Zhou, Y. Materials Chemistry for Sustainability and Energy. *J. Chem.* **2014**, *2014*, 1–3. [[CrossRef](#)]

27. Gokhale, S.; Ahmed, N.; Mahamuni, S.; Rao, V.; Nigavekar, A.; Kulkarni, S. XPS and XRD investigations of Dy/Si interface. *Surf. Sci.* **1989**, *210*, 85–98. [[CrossRef](#)]
28. Rydberg, S.; Engholm, M.; Rydberg, S.; Engholm, M. Charge transfer processes and ultraviolet induced absorption in Yb:YAG single crystal laser materials Charge transfer processes and ultraviolet induced absorption in Yb:YAG single crystal laser materials. *J. Appl. Phys.* **2013**, *11*, 223510. [[CrossRef](#)]
29. Sharma, S.; Brahme, N.; Bisen, D.P.; Dewangan, P. Cool white light emission from Dy³⁺ activated alkaline alumino silicate phosphors. *Opt. Express* **2018**, *26*, 29495–29508. [[CrossRef](#)]
30. Sun, J.; Zhang, X.; Xia, Z.; Du, H. Synthesis and luminescence properties of novel LiSrPO₄:Dy³⁺ phosphor. *Mater. Res. Bull.* **2011**, *46*, 2179–2182. [[CrossRef](#)]